MRI-Compatible Cascaded Blood Pressure Microsensor

1st Lodewijk Arntzen
THUAS, Delft, NL
l.h.arntzen@hhs.nl

2nd Daan Boesten
THUAS, Delft, NL
d.boesten@hhs.nl

3th Urs Wyder
Fontys, Eindhoven, NL,
u.wyder@fontys.nl

4th Jan Bernards
Fontys, Eindhoven, NL,
j.bernards@fontys.nl

5th Paolo Sberna
TUD, Delft, NL
P.M.Sberna@tudelft.nl

6th Francesco Stallone
TUD, Delft, NL
f.s.stallone@tudelft.nl

7th Hande Aydogmus
TUD, Delft, NL
h.aydogmus@tudelft.nl

8th Remco Nieuwland
Somni B.V., Delft, NL
remco.nieuwland@somnisolutions.com

9th Marinus van der Hoek
VanderHoek B.V., Vlaardingen, NL,
mj@vanderhoekphotonics.com

10th Henk van Zeijl
TUD, Delft, NL
H.W.vanZeijl@tudelft.nl

11th Jan Schreuder
CDLeycom, Hengelo, NL
j.schreuder@cdleycom.com

12th Guust van Liere
Unitron, IJzendijke, NL
g.vanliere@unitron-group.com

13th John Bolte
THUAS, Delft, NL,
J.F.B.bolte@hhs.nl

***Abstract*—For the prevention and diagnosis of cardiovascular diseases, the ability to measure cardiac performance is of great importance. A new type of sensor compatible for catheterization is proposed that can diagnose cardiovascular performance while being immune to Electromagnetic Interference (EMI), as well as compatible with Magnetic Resonance Imaging (MRI), with the ability to expand the number of sensors on a single catheter without additional wires. A prototype consisting of three cascaded pressure sensors on a single optical fiber has been fabricated, allowing measurements of important local medical indicators, such as Fractional Flow Reserve (FFR). The fabricated sensor is able to measure blood pressure with a resolution of 3.6 mmHg at a rate of 2 kHz, with room for improvement. Although further work is needed in the miniaturization and integration of the sensor in a catheter, preliminary measurements show promising results.**

***Index Terms*—cardiovascular diseases; blood pressure sensor; MRI-compatible; optical fiber; catheter.**

I. Introduction

In 2020, in the Netherlands alone, 233,808 reported hospitalizations due to cardiovascular disease were reported [1]. In that same year, a total number of 36,579 people died as a result of cardiovascular disease, representing 22% of the total mortality. For the diagnosis and prevention of cardiovascular disease, measurements of cardiac performance are of considerable importance. To improve diagnostics, accurate and reliable measurements are critical; for example, to determine cardiac output, Pressure-Volume (PV) curves are often measured with piezo-based pressure sensor arrays on a catheter tip. Measuring pressure in arrays allows measurement of other important local medical indicators, such as FFR [2]. These indicators are essential for medical diagnosis, and are currently standard procedure. However, one of the central problems of piezo sensors is that the detection technique is based on electrical signals, which limits precision and reliability due to high static magnetic fields and EMI. Moreover, it is highly desirable that future detection techniques can combine diagnostic capabilities with MRI [4]. This implies that the performance of the sensor must be independent of high magnetic fields, up to 7 Tesla [5]. A different approach was chosen using integrated optics [3] for the development of a new generation of catheter sensors. Furthermore, it is desired that the sensor is suitable for catheters with a diameter of 6 Fr ($\approx$ 2 mm) or less, and a pressure resolution of 1 mmHg or less. The working principle is based on a single optical fiber consisting of multiple Fiber Bragg Gratings (FBG) separated by any adjustable spacing. Combined with an interrogator, the FBGs measure a shift in near-infrared electromagnetic wavelength proportional to the deformations of a Silicon Nitride (Si_3N_4) membrane at varying pressures.

II. Theory

In fluid dynamics, the most simple form of Bernoulli's Law states

$$P + \frac{1}{2}\rho v^2 = \text{Constant}, \tag{1}$$

where P refers to the static pressure, and $\frac{1}{2}\rho v^2$ refers to the dynamic pressure. This equation is easily derived directly from energy conservation. It implies that a cascade of microscaled pressure sensors can be used to trace stenosis in a blood vessels, as visualized in Figure 1. It also implies that such a cascade is suitable for verifying correct positioning of a stent after surgery - since correct stent positioning would directly cause vanishing blood pressure difference over the stenosis. Poisseuille-Hagen law describes the pressure difference over a cylindrical tube of length L, of a fluid in laminar fluid flow

$$\Delta P = \frac{8\mu L Q}{A^2}, \tag{2}$$

where Q refers to the flowrate [$\frac{\mathrm{m}^3}{\mathrm{s}}$], A [m^2] the cross-

 ISBN: 978-1-68558-083-4

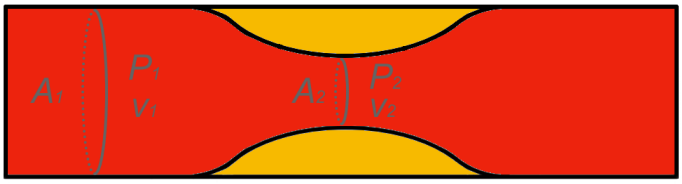

Fig. 1. Bernoulli states a direct relation between cross-sectional areas A_1 and A_2, static pressures P_1 and P_2, and flow speeds v_1 and v_2. If the area reduces, the static pressure reduces, while the dynamic pressure ($\frac{1}{2}\rho v^2$) increases. This implies that a cascaded pressure sensor can be used to trace stenosis in a blood vessel.

sectional area of the cylindrical tube, and μ [Pa · s] the dynamical viscosity. The assumptions in the derivations set some limitations using (1) and (2), but the equations are illustrative for additional applications of a cascaded microscaled pressure sensor. For instance, the proportion of red blood cells in the blood (hematocrit) correlates with the viscosity. An increase of hematocrit leads to a higher viscosity. On average, blood has a viscosity of approximately three times that of water, meaning that the driving pressure to pump blood through the vessels is higher. Polycythemia (or Erythrocytosis) is an anomaly leading to a enlarged hematocrit that can reach up to 70% [7]. The viscosity of the blood will then be up to ten times larger than that of water, making it harder for the heart to pump blood through the vascular system. Equation (2) shows that a cascade of pressure sensors fitted in a catheter show an abnormal pressure decline over the cascade. Additional diagnostic detection is possible, if the sensor cascade has sufficient dynamical response. In that case, it will be possible to analyze the arterial pulse in the time domain, revealing the performance of the heart and vessels [8]. A typical example of a study performed exploring pressure curves with a high precision, is shown in Figure 2. This example shows that analysing the exact shape of the pressure wave can be used as a diagnostic tool.

III. Finite Element Modeling

To verify the feasibility of the sensor, a simulation of the Si_3N_4 membrane was performed using a Finite Element Method (FEM) analysis. In this simulation, the behavior of membranes with thicknesses ranging from 200 to 400 nm was studied under different loading conditions. Calculated deformations of the membranes varied typically from 1.5 to 2.5 micrometers at pressures from 50 mmHg to 200 mmHg, respectively. Given the strain sensitivity of optical fibers with low bend loss, these values are within the measurement range of commonly available optical fibers and interrogators [10] [9]. The FEM model and resulting deformation at a pressure of 200 mmHg is shown in Figure 3.

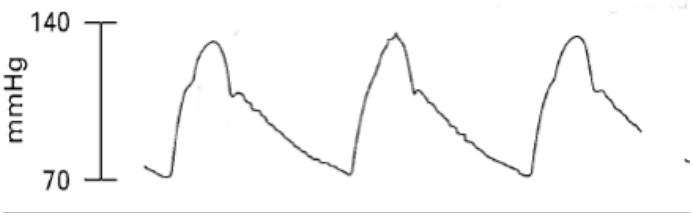

Fig. 2. Typical example of pressure time domain analysis. Analysing the exact shape and properties, can be used as an diagnostic tool. Adapted from: [8].

IV. Fabrication

The fabrication of the sensor device consists of the fabrication of the Si_3N_4 membrane using photolithographic processes and the adhesion of the FBG to the Si_3N_4 membrane.

A. Microfabrication of the Silicon Nitride Membrane

For the microfabrication of the Si_3N_4 membrane, a $300\,\mu m$ double side polished p-type (boron) Silicon wafer with a $<100>$ orientation is used. Using Low Pressure Chemical Vapour Deposition (LPCVD) with a mixture of NH_3 and H_2SiCl_2, a thin film of Si_3N_4 is deposited on both sides of the substrate. Si_3N_4 was chosen because of its relatively high flexiblity and low etch rate compared to Silicon. The thickness of the deposited Si_3N_4 thin film was measured using an Woollam M-2000 Ellipsometer at a value of $399.47\,nm$. The stress of the thin film was measured with the use of a Flexus 2320-S thin-film stress measurement instrument at a value of $337.73\,MPa$. The wafer with a thin film of Si_3N_4 is shown in Figure 4, left.

Using an ASML PAS 5500/60 stepper, rectangular patterns representing the membranes are exposed on a layer of photoresist that is deposited to the backside of the wafer. The exposed patterns are etched away using a Drytek Triode 384T plasma etcher with a mixture of 90% C_2F_6 and 10% Cl_2 until the bare silicon of the wafer remains. The resulting exposed patterns are shown in Figure 4, right. A cavity is created by placing the wafer in a bath of distilled water with 30% potassium hydroxide (KOH) until the silicon is completely etched and only the thin Si_3N_4 layer on the topside of the wafer remains. The silicon wafer with an orientation of $<100>$ etches faster than in the $<111>$ orientation, resulting in a V-shaped cavity with an angle of $54.7\,degrees$. The cavity, combined with the thin layer of Si_3N_4, acts as a pressure chamber that deforms dependent on the loading conditions. The Si_3N_4 membrane has dimensions of 2.0x0.3 mm. Lastly, the wafer is diced using a diamond saw resulting in rectangular chips with a size of 10x2.5x0.3 mm (LWH).

B. Adhesion of Silicon Nitride Membrane and FBG

As shown in Figure 3, the deformation of the Si_3N_4 membrane is the highest in the center of the membrane. Thus, it is

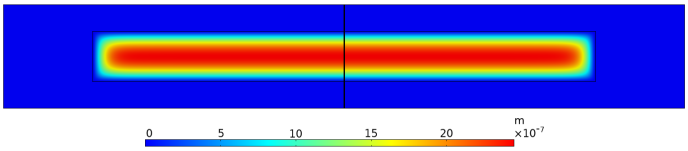

Fig. 3. FEM model of the Si_3N_4 membrane showing the deformation at an applied pressure of 200 mmHg.

 ISBN: 978-1-68558-083-4

Fig. 4. Left: Wafer with a Si_3N_4 thin film. Right: Wafer with exposed patterns representing the membranes.

important to align the FBG precisely at the center of the Si_3N_4 membrane. For this purpose, an alignment setup is made consisting of clamps for the optical fiber, a chip housing and an XYZ micromanipulator with a precision scale of $1.0\,\mu m$ for the positioning of the optical fiber on top of the membrane. The chip housing is made using an Stereolithography (SLA) 3D printer, and is shown in Figure 5. The aligned optical fiber is bonded to the Si_3N_4 membrane using an UV-curable adhesive with low shrinkage properties [11].

V. Measurement Setup

The chip housing not only holds the rectangular chips with the Si_3N_4 membrane in place, but also has a built-in provision for Luer locks for connecting pressure input and output hoses. The Luer locks allow multiple pressure sensors to be connected together so that pressure changes can be measured simultaneously at multiple points along the optical fiber. The measurement device with three fabricated pressure sensors in cascade is shown in Figure 6. The optical fiber is connected to a FAZT I4G interrogator that measures the wavelength shift of the FBGs at a measurement frequency of 2 kHz with precision of less than 0.1 pm [10]. Blood pressure signals are generated with a Biotek Fluke 601A Blood Pressure System Calibrator that is connected to the measurement device. This device can emulate heart rhythms at different systolic and diastolic blood pressure values.

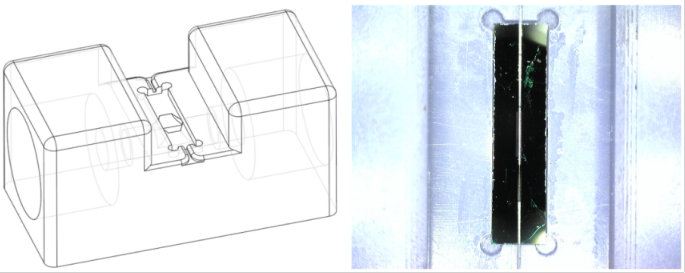

Fig. 5. Left: CAD drawing of the chip housing. Right: 3D printed chip housing with an FBG aligned on top of the Si_3N_4 membrane.

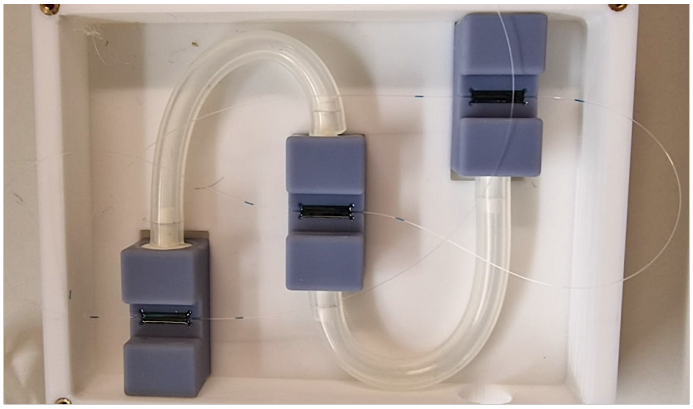

Fig. 6. Measurement device consisting of three cascaded pressure sensors, each on a chip housing, with a single optical fiber.

VI. Performance and Results

The characteristics and performance of the three fabricated blood pressure sensors were determined by applying various loading conditions and measuring the wavelength shift relative to a steady state at 0 mmHg. An Atrial tachycardia heart rhythm at a systolic blood pressure of 140 mmHg and a diastolic blood pressure of 80 mmHg at a frequency of 120 BPM was applied to the measurement device, the result of which is shown in Figure 7. The average wavelength shift of the three sensors is measured at a value of 0.83 $\pm$ 0.05 pm due to a pressure change of 60 mmHg, resulting in a sensor resolution of 3.6 mmHg with the use of an FAZT I4G interrogator. The dynamic response of the sensors is measured at a resolution smaller than $50\,ms$.

VII. Conclusion

In this study, an MRI-compatible cascaded blood pressure sensor suitable for catheterization was designed, fabricated, and characterized. The dynamic response of the sensors

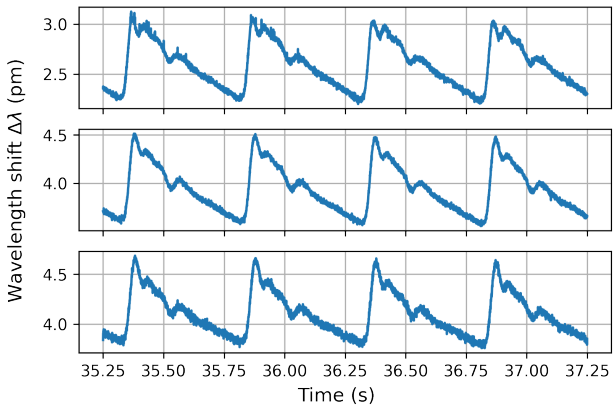

Fig. 7. Performance of the cascaded pressure sensors on a single optical fiber. An Atrial tachycardia heart rhythm was emulated at a systolic blood pressure of 140 mmHg and diastolic blood pressure of 80 mmHg at a frequency of 120 BPM.

 ISBN: 978-1-68558-083-4

was characterized by applying an emulated atrial tachycardia cardiac rhythm at a systolic blood pressure of 140 mmHg and a diastolic blood pressure of 80 mmHg at a frequency of 120 BPM. The dynamic response (measured at smaller than $50\,\mathrm{ms}$) is sufficient to see the specific characteristics in the blood pressure wave. This is an important requirement for determining the suitability of the sensor to measure the performance of the heart and vessels.

The average wavelength shift of the three cascaded sensors is measured at a value of 0.83 $\pm$ 0.05 pm shift as a result of a pressure change of 60 mmHg, translating to an average sensor resolution of 3.6 mmHg with the use of an FAZT I4G interrogator. Further work is needed to increase the sensitivity of the sensors to the desired resolution of 1 mmHg. This could be achieved by increasing the deformation of the Si_3N_4 membrane per unit pressure, for example, by increasing the width of the membrane.

To achieve the desired catheter diameter of 6 Fr ($\approx$ 2mm) or less, further miniaturization efforts are required to reduce the size of the chip containing the Si_3N_4 membrane, i.e., by reducing the size of the silicon substrate surrounding the membrane. In addition, future work is planned to the integration of the sensor design into a catheter.

Although preliminary measurements were done to verify the compatibility of the sensors in magnetic fields up to 1.3 T, no measurements have been done yet to verify compatibility with high magnetic fields used in MRI scans. Future measurements are planned to experimentally prove that the fabricated sensor is compatible with the high magnetic fields used in MR imaging.

ACKNOWLEDGMENT

Funding provided by the SIA MKB-RAAK program. We would like thank former Bachelor Physics students Dorus Elstgeest, Lennart van der Hengel, Huib Dijkstra, Nils Boertjes, Lea Visscher, Iris van der Heide and Esther Pot for their dedicated experimental work as well as FEM simulations.

REFERENCES

[1] Hartstichting, "Hart- en vaatziekten in Nederland 2021", pp. 4-27, Dec 2021, https://hartstichting-hartstichting-portal-p01.s3.eu-central-1.amazonaws.com/s3fs-public/2022-11/hart-en-vaatziekten-nederland-cijfers-2021.pdf?, retrieved: Feb 2023

[2] Kathinka Peels, Nico H.J. Pijls, and Bernard de Bruyne. "Measurement of fractional flow reserve to assess the functional severity of coronary-artery stenoses", Jun 1996, publisher: N Engl J Med

[3] Fiber Bragg Grating Strain Sensor Incorporated to Monitor Patient Vital Signs During MRI, 4986, VOL. 13, NO. 12, Dec 2013, publisher: IEEE

[4] Andreas Kumar, David J. Patton, and Matthias G. Friedrich, "The emerging clinical role of cardiovascular magnetic resonance imaging", Jun 2010, publisher: Pulsus Group

[5] UMC Utrecht, "7T-MRI" https://www.umcutrecht.nl/nl/wetenschappelijk-onderzoek/7t-mri, retrieved: Feb 2023.

[6] "Venturi Effect", https://en.wikipedia.org/wiki/Venturi_effect, retrieved: Feb 2023.

[7] John E. Hall, "Guyton and Hall Textbook of Medical Physiology", pp. 155-166, 2003.

[8] O'Rourke, M.F., "Time domain analysis of the arterial pulse in clinical medicine", Med Biol Eng Comput 47, pp. 119–129, Feb 2009, publisher: IFMBE

[9] FBGS, Draw Tower Gratings, Overview, https://fbgs.com/components/draw-tower-gratings-dtgs/, retrieved: Feb 2023.

[10] Femto Sensing International, FAZT I4G INTERROGATOR Datasheet, https://femtosensing.com/wp-content/uploads/2020/01/FSI-FAZ-I4G-Interrogator-Datasheet-V4.pdf, retrieved: Feb 2023.

[11] Norland Products, Norland Optical Adhesive 65 Technical Datasheet, https://www.norlandprod.com/adhesives/NOA%2065.html, retrieved: Feb 2023.

 ISBN: 978-1-68558-083-4